J Low Temp Phys (2008) 153: 304–324
DOI 10.1007/s10909-008-9826-2

The Vortex State and Josephson Critical Current of a Diffusive SNS Junction

F.S. Bergeret · J.C. Cuevas

Received: 22 May 2008 / Accepted: 20 August 2008 / Published online: 7 October 2008

Abstract We study theoretically the electronic and transport properties of a diffusive superconductor-normal metal-superconductor (SNS) junction in the presence of a perpendicular magnetic field. We show that the field dependence of the critical current crosses over from the well-known Fraunhofer pattern in wide junctions to a monotonic decay when the width of the normal wire is smaller than the magnetic length $\xi_H = \sqrt{\Phi_0/H}$, where H is the magnetic field and Φ_0 the flux quantum. We demonstrate that this behavior is intimately related to the appearance of a linear array of vortices in the middle of the normal wire, the properties of which are very similar to those in the mixed state of a type II superconductor. This novel vortex structure is also manifested in a strong modulation of the local density of states along the transversal dimension, which can be measured with existing experimental techniques.

PACS 74.45.+c · 74.50.+r · 74.25.Qt

1 Introduction

When a Josephson tunnel junction is subjected to a perpendicular magnetic field, the superconducting phase difference varies along the barrier splitting up the junction into regions in which the current through it has opposite signs, and the critical current is thus greatly reduced [1]. In the case of a rectangular and uniform tunnel junction, the field dependence of the critical current is given by a Fraunhofer diffraction pattern formula, which in particular means that the supercurrent vanishes every time that the magnetic flux enclosed in the junction, Φ, is a multiple of the flux quantum

F.S. Bergeret (✉) · J.C. Cuevas
Departamento de Física Teórica de la Materia Condensada, Universidad Autónoma de Madrid, 28049 Madrid, Spain
e-mail: fs.bergeret@uam.es

$\Phi_0 = h/2e$. This effect was first observed by Rowell [2] in the context of tunnel junctions and since then it has been reported in many other weak links [3, 4]. In particular, this behavior has also been found by many authors in the case of diffusive SNS junctions [5–10], where the Josephson coupling is established by the so-called *proximity effect* [11], in which Cooper pairs from the superconducting banks diffuse into the normal metal. In this sense, it came to a surprise the recent experimental results of Angers *et al.* [12] that showed that diffusive junctions with dimensions comparable or smaller than the superconducting coherence length exhibit a monotonic decay of the critical current with magnetic field, i.e. the absence of magnetic interference patterns. These puzzling results have motivated us to revisit the question of what is the magnetic field dependence of the critical current of diffusive SNS junctions [13]. The goal of this work is provide a detailed answer to this question.

It is worth mentioning that the influence of the width of the normal wire in the shape of interference patterns of SNS junction has already been discussed in the context of ballistic junctions. A few years ago, Heida *et al.* [14] measured the critical current as a function of a perpendicular magnetic field in ballistic SNS junctions of comparable length and width and found a periodicity close to $2\Phi_0$, instead of the standard Φ_0 of the Fraunhofer pattern. This was qualitatively explained in Refs. [15, 16] in terms of the classical trajectories associated with current-carrying Andreev states in a normal clean wire.

In Ref. [13] we have shown that the resolution of the experimental puzzled explained above is intimately related to the issue of the formation of a magnetic vortex structure in the normal conductor. Since Abrikosov's prediction of the existence of vortices in type II superconductors [17, 18], their physics has attracted a huge attention in the last five decades. In particular, vortex matter in mesoscopic superconductors has been an active field in the last years [19]. It has been shown that basic properties such as critical fields [20] and the magnetization [21] depend crucially on the size and topology of mesoscopic samples, which in turn determine the vortex structure. There is also a great interest in the study of nucleation of superconductivity and vortex matter in hybrid structures [22]. However, little attention has been paid to the formation of vortices inside non-superconducting materials. Our goal here is to answer the following fundamental questions: Is it possible to induce a vortex structure in a normal wire by proximity to a superconductor? If so, what are the properties of such *proximity vortices* and their influence on the dc Josephson effect?

The relation between the behavior of a Josephson junction in a magnetic field and that of type II superconductor has been discussed by many authors. Such relation depends on the transverse dimensions of the weak link, the normal wire in our case, relative to the so-called Josephson penetration depth, which is given by $\lambda_J = \sqrt{\hbar/2\mu_0 e j_c d}$, where j_c is the critical current per unit area and d is the effective length of the junction including the London penetration depths in the leads. This length scale is of the order of 1 mm in ordinary tunnel junctions. In the case in which the width of the junction is smaller than λ_J, which is the limit of interest for this work, the Josephson currents are unable to screen the external magnetic field. In this case, as explained above, the local value of the Josephson current oscillates sinusoidally with the position along the junction transverse direction alternating its sign. The net current cancels to zero over each complete cycle. These cycles are sometimes referred to as "Josephson vortices" because they carry no net current [4], but it must be

stressed that they do not share other properties with the Abrikosov vortices. Finally, the presence of these "vortices" gives rise to the Fraunhofer pattern. In the case in which the transversal dimensions are larger than λ_J and for weak applied fiels, the supercurrent tends to screen the field from the interior of the junction. Then, above some critical field, flux completely penetrates the junction, but the Josephson vortices are no longer sinusoidal. Instead, they acquire a solution character forming a one-dimensional vortex-like structure, whereas in a type II supeconductor Abrikosov vortices form a two-dimensional lattice. But again, the nature of the vortex is also different, since there is no normal core. For a detailed discussion of this latter limit see Chap. 5 of Ref. [3] and Ref. [23].

In order to answer the questions posed above, in this work we study theoretically the supercurrent of a diffusive SNS junction in the presence of a perpendicular magnetic field, H. By solving the full two-dimensional Usadel equations [24], we are able to describe the condensate function induced in the normal region as well as the critical current for arbitrary length (L), width (W), temperature and quality of the SN interfaces. We find that when W is smaller than the magnetic length defined as $\xi_H = \sqrt{\Phi_0/H}$, the field just acts as a pair-breaking mechanism that supresses monotonically the superconductivity in the normal wire. This implies in practice that the critical current decays roughly in a exponential manner with the field and thus, there is no interference pattern. As the width increases we find the appearance of a linear array of vortices located exactly in the middle of the normal wire. These vortices have similar properties to those in the mixed state of a type II superconductor [17, 18]. In particular, they exhibit normal cores, circulating currents around the cores and quantization of the circulation of the phase of the superconducting correlations. The consequence of this vortex structure is the appearance of an interference pattern in the critical current that tends to the Fraunhofer pattern in the wide-junction limit ($W \gg L, \xi_H$). This peculiar vortex structure is also manifested in a strong modulation of the local density of states (DOS) in the normal wire. As one moves along the transversal direction, the local DOS becomes that of the normal state in the center of the vortices and exhibits a minigap between them, which depends on the value of local gauge-invariant superconducting phase difference and on the Thouless energy $\epsilon_T = \hbar D/L^2$, where D is the diffusion constant. This local DOS constitutes an unambiguous signature of the existence of this novel vortex structure and it is amenable to measurements with the existent experimental techniques.

The rest of the paper is organized as follows. In the next section we present the general formalism based on the quasiclassical theory of superconductivity, which will be used throughout this work to compute the electronic and transport properties of diffusive SNS junctions. Then, in Sect. 3 we study the limit of weak proximity effect, where the general equations can be greatly simplified and one can obtain analytical results for both the vortex structure and the critical current in different limits. Section 4 is devoted to the analysis of highly transparent junctions. In this case, we concentrate ourselves in the analysis of the local density of states and pair correlations in the normal wire and in the magnetic field dependence of the critical current for arbitrary aspect ratio. Finally, we conclude in Sect. 5 by summarizing our main results, discussing their comparison with recent experiments and proposing the realization of new ones to confirm our predictions.

2 The Quasiclassical Formalism

We consider a SNS junction as the one depicted in Fig. 1, where N is a diffusive normal metal of length L and width W coupled to two identical superconducting reservoirs with an energy gap Δ. The normal film lies in the xy-plane, where $x \in [0, L]$ and $y \in [-W/2, W/2]$ and is subjected to an uniform external field $\mathbf{H} = H\hat{z}$ perpendicular to the film. For the sake of simplicity, we assume that the thickness of the normal wire is smaller than the London penetration depth, which implies that the field penetrates completely in the normal region. We also neglect both the suppression of the pair potential in the leads near the interfaces and the inelastic interactions in the normal wire. Additionally, we shall assume that the field does not affect the superconductivity in the electrodes.

In order to describe the electronic and transport properties of these junctions we use the quasiclassical theory of superconductivity in the diffusive limit [24, 25], where the mean free path is much smaller than the superconducting coherence length in the normal metal, $\xi = \sqrt{\hbar D/\Delta}$, where D is the diffusion constant. Since we shall only deal with equilibrium quantities, this theory can be formulated in terms of momentum averaged retarded Green's function $\hat{G}^R(\mathbf{R}, \epsilon)$, which depends on position $\mathbf{R}$ and an energy argument ϵ. This propagator is a 2×2 matrix in electron-hole (Nambu) space

$$\hat{G}^R = \begin{pmatrix} g^R & f^R \\ \tilde{f}^R & \tilde{g}^R \end{pmatrix}, \tag{1}$$

which satisfies the stationary Usadel equation, which in the N region reads [25]

$$\frac{\hbar D}{\pi} \nabla \cdot (\hat{G}^R \check{\nabla} \hat{G}^R) + \epsilon[\hat{\tau}_3, \hat{G}^R] = \frac{ieD}{\pi} \mathbf{A} \cdot [\hat{\tau}_3, \hat{G}^R \check{\nabla} \hat{G}^R]. \tag{2}$$

Here, $\mathbf{A}$ is the vector potential, $\check{\nabla} = \nabla \hat{1} - (ie/\hbar)\mathbf{A}\hat{\tau}_3$ and $\hat{\tau}_3$ is the Pauli matrix in electron-hole space. In the previous equation we have already used the Coulomb gauge $\nabla \cdot \mathbf{A} = 0$. Equation (2) is supplemented by the normalization condition $(\hat{G}^R)^2 = -\pi^2 \hat{1}$. In general, the Usadel equation has to be solved together with the Maxwell equation $\nabla \times \mathbf{H} = \mu_0 \mathbf{j}$ in a self-consistent manner. However, we are interested here in the case where the width W is smaller than the Josephson penetration length λ_J. In this case, one can ignore the screening of the magnetic field by the Josephson currents and the field is equal to the external one (for a discussion of this issue, see Ref. [3]). Finally, we have to provide the boundary conditions for (2).

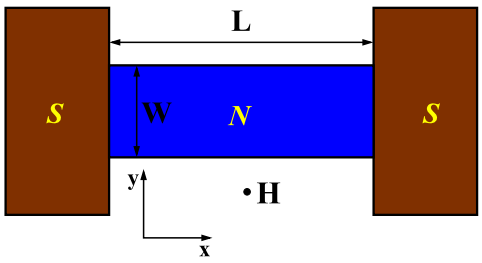

Fig. 1 (Color online) Top view of the diffusive SNS junction under consideration, where the normal wire has a length L and a width W. The wire thickness is assumed to be much smaller than the London penetration depth. The magnetic field is applied perpendicular to the plane of the page ($\mathbf{H} = H\hat{z}$)

For the two SN interfaces we use the boundary conditions introduced in Refs. [26, 27], which allow us describing the system for arbitrary transparency of the interfaces. These conditions for an spin-conserving interface are expressed in terms of the Green's functions as follows

$$r\hat{G}^R_\beta\left(\partial_x\hat{1}-\frac{ie}{\hbar}A_x\hat{\tau}_3\right)\hat{G}^R_\beta=\frac{2\pi^2[\hat{G}^R_\beta,\hat{G}^R_\alpha]}{4\pi^2-\tau(\{\hat{G}^R_\beta,\hat{G}^R_\alpha\}+2\pi^2)}, \tag{3}$$

where $\hat{G}^R_{\beta(\alpha)}$ refers to the retarded Green's functions on side $\beta(\alpha)$ of the interface and τ is the normal transmission coefficient of the interface conduction channels. Here, we assume that all the channels have the same transparency and define $r=G_{\rm N}/G_{\rm B}$ as the ratio between the normal state conductance of the wire, $G_{\rm N}$, and the conductance of the barriers, $G_{\rm B}$, which we assume to be identical. For the case of transparent interfaces, i.e. for $r=0$, these conditions simply reduce to the continuity of Green's functions in both SN interfaces. On the other hand, for the metal-vacuum lower and upper borders in the normal wire, the appropriate conditions are

$$\left(\partial_y\hat{1}-\frac{ie}{\hbar}A_y\hat{\tau}_3\right)\hat{G}^R|_{y=\pm W/2}=\hat{0}, \tag{4}$$

which simply express the fact that the current density in the y-direction vanishes at the edges of the sample.

We are interested in different physical properties that can be conveniently expressed in terms of the quasiclassical Green's functions. For instance, the local density of states (DOS) is given by $\rho(\mathbf{R},\epsilon)=-\mathrm{Im}\{g^R(\mathbf{R},\epsilon)\}/\pi$. In order to quantify the superconducting correlations in the normal wire, we introduce the pair correlation function defined as

$$\Psi(\mathbf{R})=\frac{1}{4\pi i}\int d\epsilon[f^R(\mathbf{R},\epsilon)-f^A(\mathbf{R},\epsilon)]\tanh(\beta\epsilon/2), \tag{5}$$

where $\beta=1/k_BT$. Notice that this quantity, apart from the attractive coupling constant, describes the pair potential in a superconductor and it is non-zero inside the normal metal due to the proximity effect. Finally, the current density, $\mathbf{j}(\mathbf{R})$, can be written in terms of the anomalous Green's functions as

$$\mathbf{j}(\mathbf{R})=\frac{\sigma_N}{4\pi^2e}\int_{-\infty}^{\infty}d\epsilon\tanh\left(\frac{\beta\epsilon}{2}\right)\mathrm{Re}\left\{f^R\nabla\tilde{f}^R-\tilde{f}^R\nabla f^R+\frac{4ie}{\hbar}\mathbf{A}f^R\tilde{f}^R\right\}, \tag{6}$$

where σ_N is the conductivity of the normal wire. The net current is finally obtained integrating j_x across the transversal direction.

At this stage the technical challenge is to solve (2). This equation is indeed a set of nonlinear second-order partial differential equations, whose resolution is a formidable task. The main problem lies in the fact that the problem is in general of two-dimensional nature, as we proceed to explain. By choosing, for instance, the gauge $\mathbf{A}=-Hy\hat{x}$, one can identify in (2) the length $\xi_{\rm H}=\sqrt{\Phi_0/H}$ as the characteristic length scale for the variation of the Green's functions in the y-direction due to the magnetic field. Therefore, if the width W is larger than $\xi_{\rm H}$, which will always occur

for sufficiently high fields, no matter how small W is, the problem becomes two-dimensional. It is worth stressing that, to our knowledge, so far the solution of the Usadel equations in 2D situations has not been reported in the literature.

In the next section we shall show that one can make a lot progress analytically in several limiting cases, but the rest of this section is devoted to explain how (2) can be solved numerically for arbitrary range of parameters. For this purpose, the first step is to introduce a suitable parametrization, which accounts automatically for the normalization condition. Our choice here is the so-called Riccati parametrization [28], in which for spin-singlet superconductors in an equilibrium situation the retarded Green's functions are parametrized in terms of two coherent functions $\gamma^R(\mathbf{R},\epsilon)$ and $\tilde{\gamma}^R(\mathbf{R},\epsilon)$ as follows

$$\hat{G}^R = \frac{-i\pi}{(1+\gamma^R\tilde{\gamma}^R)}\begin{pmatrix} 1-\gamma^R\tilde{\gamma}^R & 2\gamma^R \\ 2\tilde{\gamma}^R & -1+\gamma^R\tilde{\gamma}^R \end{pmatrix}. \tag{7}$$

Using these definitions and the Usadel equation (2), one can obtain the following equations for γ^R and $\tilde{\gamma}^R$ in the normal wire region [29]

$$\begin{aligned} \left(\nabla - \frac{2ie}{\hbar}\mathbf{A}\right)^2\gamma^R + \frac{\tilde{f}^R}{i\pi}\left[\left(\nabla - \frac{2ie}{\hbar}\mathbf{A}\right)\gamma^R\right]^2 &= -2i\frac{\epsilon}{\hbar D}\gamma^R, \\ \left(\nabla + \frac{2ie}{\hbar}\mathbf{A}\right)^2\tilde{\gamma}^R + \frac{f^R}{i\pi}\left[\left(\nabla + \frac{2ie}{\hbar}\mathbf{A}\right)\tilde{\gamma}^R\right]^2 &= -2i\frac{\epsilon}{\hbar D}\tilde{\gamma}^R. \end{aligned} \tag{8}$$

Notice that the equation for $\tilde{\gamma}^R$ can be obtained from the equation for γ^R by exchanging γ^R by $\tilde{\gamma}^R$ (and vice versa) and changing the sign of the vector potential. If we choose now the gauge $\mathbf{A} = -Hy\hat{x}$ and introduce the dimensionless coordinates $\tilde{x} \in [0,1]$ and $\tilde{y} \in [-1/2, 1/2]$, we can write the previous equations in the following explicit form

$$\begin{aligned} &\partial_{\tilde{x}}^2\gamma^R + \left(\frac{L}{W}\right)^2\partial_{\tilde{y}}^2\gamma^R - \frac{2\tilde{\gamma}^R}{1+\gamma^R\tilde{\gamma}^R}\left([\partial_{\tilde{x}}\gamma^R]^2 + \left(\frac{L}{W}\right)^2[\partial_{\tilde{y}}\gamma^R]^2\right) \\ &\quad + 4is\tilde{y}\left(\frac{1-\gamma^R\tilde{\gamma}^R}{1+\gamma^R\tilde{\gamma}^R}\right)\partial_{\tilde{x}}\gamma^R - 4s^2\tilde{y}^2\left(\frac{1-\gamma^R\tilde{\gamma}^R}{1+\gamma^R\tilde{\gamma}^R}\right)\gamma^R = -2i\frac{\epsilon}{\epsilon_{\mathrm{T}}}\gamma^R. \end{aligned} \tag{9}$$

Here, we have defined the parameter $s = \pi\Phi/\Phi_0$, where $\Phi = HLW$ is the flux enclosed in the junction. There is a second equation for $\tilde{\gamma}^R$ that can be obtained from this one by doing the replacements explained above.

Finally, we have to specify the boundary conditions for these coherent functions. For the two SN interfaces, the conditions of (3) can be expressed in terms of the coherent functions as follows

$$\begin{aligned} &r\frac{\partial_{\tilde{x}}\gamma_\beta^R + (\gamma_\beta^R)^2\partial_{\tilde{x}}\tilde{\gamma}_\beta^R - 2is\tilde{y}\gamma_\beta^R(1-\gamma_\beta^R\tilde{\gamma}_\beta^R)}{(1+\gamma_\beta^R\tilde{\gamma}_\beta^R)^2} \\ &\quad = \frac{(1-\gamma_\beta^R\tilde{\gamma}_\beta^R)\gamma_\alpha^R - (1-\gamma_\alpha^R\tilde{\gamma}_\alpha^R)\gamma_\beta^R}{(1+\gamma_\beta^R\tilde{\gamma}_\beta^R)(1+\gamma_\alpha^R\tilde{\gamma}_\alpha^R) - \tau(\gamma_\alpha^R-\gamma_\beta^R)(\tilde{\gamma}_\alpha^R-\tilde{\gamma}_\beta^R)}. \end{aligned} \tag{10}$$

This equation is coupled to a second one obtained by making the replacements explained above. The conditions of (4) for the borders of the normal wire adopt now the simple form:

$$\partial_{\tilde{y}}\gamma^R|_{\tilde{y}=\pm 1/2} = \partial_{\tilde{y}}\tilde{\gamma}^R|_{\tilde{y}=\pm 1/2} = 0. \tag{11}$$

Equation (9) and the corresponding one for $\tilde{\gamma}^R$ form a set of coupled second-order nonlinear differential equations, whose general solution is not possible to obtain analytically. In order to solve them numerically, we have adapted the so-called relaxation method for boundary value problems [30] to the case of partial differential equations. Briefly, the idea goes as follows. We first discretize the equations by using finite differences. The corresponding algebraic nonlinear system is then solved using the Newton-Raphson method [30]. In this method a nonlinear system of equations is solved iteratively until convergence. One starts with a guess for the solution and it is updated in every step with the solution of the corresponding linearized system [30]. The key problem here is the huge dimension of these linear systems. To give an idea, let us say that we want to use a fine grid of 100×100 points to describe our two-dimensional system. This means that one has to solve a set of 10^4 equations. Moreover, one has to do it several thousand times to integrate the current density for a particular value of the phase difference and magnetic field. What finally makes the resolution possible at all is the fact that the algebraic system resulting from the discretization is a block-tridiagonal system that can be solved very efficiently using special algorithms of linear algebra such as the so-called Thomas algorithm.

3 Weak Proximity Effect

In the limit of very low transparent interfaces (tunnel barriers), or for temperatures close to the superconducting critical temperature, the anomalous Green's functions are small and one can linearize the Usadel equation (2). It is convenient for the subsequent analysis to use Matsubara-Green's functions, which can be easily obtained by making the substitution in all the equations of the previous section: $\epsilon \to i\omega_n$, where $\omega_n = \pi k_B T(2n+1)$ are the Matsubara energies.

In this weak proximity limit the Green's functions can be approximated by (see (1))

$$\hat{G}(\omega_n) \approx \begin{pmatrix} 1 & f(\omega_n) \\ \tilde{f}(\omega_n) & -1 \end{pmatrix}. \tag{12}$$

The functions f and $\tilde{f}$ fulfill the following linearized equations which for the gauge $\mathbf{A} = -Hy\hat{x}$ are obtained from (9):

$$\partial_{\tilde{x}}^2 f + \left(\frac{L}{W}\right)^2 \partial_{\tilde{y}}^2 f + 4is\tilde{y}\partial_{\tilde{x}} f - 4s^2\tilde{y}^2 f = 2\frac{|\omega_n|}{\epsilon_T} f, \tag{13}$$

$$\partial_{\tilde{x}}^2 \tilde{f} + \left(\frac{L}{W}\right)^2 \partial_{\tilde{y}}^2 \tilde{f} - 4is\tilde{y}\partial_{\tilde{x}} \tilde{f} - 4s^2\tilde{y}^2 \tilde{f} = 2\frac{|\omega_n|}{\epsilon_T} \tilde{f}. \tag{14}$$

Notice that now the equations for f and $\tilde{f}$ are uncoupled and have an almost identical form. The linearized boundary conditions at the SN interfaces for the previous equations can be written as

$$\mp r(\partial_{\tilde{x}} f_\beta - 2is\tilde{y} f_\beta) = f_\alpha; \qquad \mp r(\partial_{\tilde{x}} \tilde{f}_\beta + 2is\tilde{y} \tilde{f}_\beta) = \tilde{f}_\alpha, \tag{15}$$

where the minus sign is for the left interface and the plus sign for the right one. Here, $f_{\beta(\alpha)}$ refers to the condensate function evaluated on side $\beta(\alpha)$ of the interfaces. As a convention we denote by α the point in the interior of the electrodes and by β the points right at the interfaces on the normal wire side. The anomalous Green's functions of the superconducting leads $\alpha = l, r$, are given by

$$f_{l,r} = f_S \exp(\pm i\phi/2); \qquad \tilde{f}_{l,r} = -f_S \exp(\mp i\phi/2), \tag{16}$$

where $f_S = i\Delta/\sqrt{\Delta^2 + \omega_n^2}$ and ϕ is the phase difference between the superconducting leads.

In the present limit of weak proximity effect, the net supercurrent through the junction can be expressed as

$$I = \left(\frac{G_N}{e}\right) \frac{i\pi k_B T}{2} \int_{-1/2}^{1/2} d\tilde{y} \sum_{\omega_n} \{\tilde{f}\partial_{\tilde{x}} f - f\partial_{\tilde{x}} \tilde{f} + 4is\tilde{y} f \tilde{f}\}. \tag{17}$$

Although (13–14) are far simpler than the original equations, it is not possible to find an analytical solution for arbitrary range of parameters and one has to resort to numerical calculations. To solve them numerically we have used finite differences to convert them in a algebraic linear system. Such system is block-tridiagonal and it can be very efficiently solved using the so-called Thomas algorithm for tridiagonal linear systems. We shall present the results of the numerical analysis for arbitrary aspect ratio in Sect. 3.3. But before, we shall concentrate in the next two subsections in the study of two limiting cases in which an analytical 1D solution can be obtained.

3.1 The Narrow-Junction Limit

In the limit in which the width W is comparable or smaller than ξ_H, the characteristic length over which the condensate function f in the normal metal varies in the transversal direction, one can average (13, 14) along the y-direction. Using that $\langle A_x \rangle_y = 0$ and $\langle A_x^2 \rangle_y = H^2 W^2/12$, it is easy to show that these equations reduce to the following one-dimensional ones

$$\partial_x^2 f - 2\left(\frac{\omega_n + \Gamma_H}{\epsilon_T}\right) f = 0; \qquad \partial_x^2 \tilde{f} - 2\left(\frac{\omega_n + \Gamma_H}{\epsilon_T}\right) \tilde{f} = 0, \tag{18}$$

where the magnetic depairing energy, Γ_H, is defined as $\Gamma_H = De^2 H^2 W^2/(6\hbar)$. If we normalize it by the Thouless energy it can be written as $\Gamma_H/\epsilon_T = (\pi\Phi/\Phi_0)^2/6$. These equations are similar to those describing the effect of spin-flip processes [31]. We have discussed in detail their solution in Ref. [32] and we just recall here the

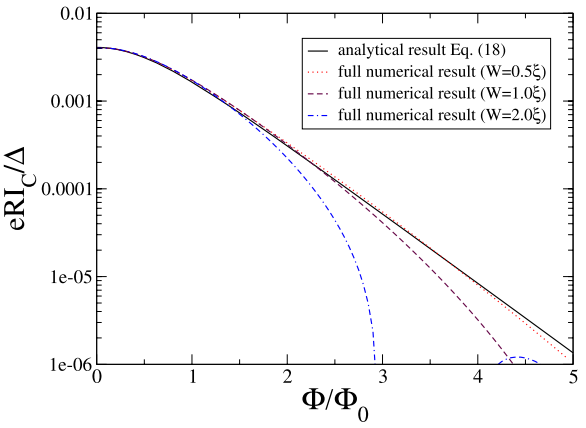

Fig. 2 (Color online) Critical current vs. magnetic flux in the weak proximity regime for a wire length $L = 8\xi$ and a temperature $k_B T = 0.01\Delta$. The *solid line* corresponds the analytical result of (19), while the *others* correspond to the exact numerical results obtained from the 2D equations for different widths, as indicated in the *legend*

result for the critical current

$$eRI_C = \frac{4\pi k_B T}{r} \sum_{n=0}^{\infty} \frac{\Delta^2/(\Delta^2+\omega_n^2)}{\sqrt{2(\frac{\omega_n+\Gamma_H}{\epsilon_T})}\sinh(\sqrt{2(\frac{\omega_n+\Gamma_H}{\epsilon_T})})}, \tag{19}$$

where we have used the fact that $R = (1+2r)/G_N \approx 2r/G_N$ for the normal resistance. In the high temperature limit, *i.e.* if $k_B T > \epsilon_T$ and for a long wire one obtains

$$eRI_C = \frac{4\pi k_B T}{r}\left(\frac{\tilde{L}}{L}\right)\exp(-L/\tilde{L}), \tag{20}$$

where the effective length $\tilde{L} = L_T L_H/\sqrt{L_T^2 + L_H^2}$. Here, $L_T = \sqrt{\hbar D/2\pi k_B T}$ is the thermal length and $L_H = \sqrt{\hbar D/2\Gamma_H}$ is the magnetic depairing length.

In Fig. 2 we show the current computed from (19) for a normal wire of a length $L = 8\xi$ (solid line). As one can see, the critical current exhibits a monotonic decay with the magnetic flux, i.e. the complete absence of interference patterns. This result is in qualitative agreement with the experiment of Ref. [12]. In this figure we also show the numerical results obtained by solving numerically the two-dimensional equations (13–14) for different widths. As expected, for the narrowest junction, $W = 0.5\xi$, the agreement is quite good in the whole range of magnetic fields. However, as the width increases and $\xi_H \sim W$, there are clear deviations from the 1D-result and, as we shall explain in detail below, one can see the appearance of interference patterns.

3.2 The Wide-Junction Limit

For a sufficiently wide junction ($W \gg \xi_H, L$) one can neglect the second term in the l.h.s. of (13–14) and the problem becomes quasi 1D since the derivatives with respect to the $\tilde{y}$-coordinate disappear. The resulting equations can be then solved analytically

and, for instance, the solution for the function f is

$$f(\tilde{x},\tilde{y}) = \frac{f_s e^{2is\tilde{y}(1-\tilde{x})}}{\pi r\lambda \sinh\lambda}[e^{-i\phi/2}\cosh(\lambda\tilde{x}) + e^{i(\phi/2-2s\tilde{y})}\cosh(\lambda(1-\tilde{x}))], \tag{21}$$

where $\lambda^2 = 2\omega_n/\epsilon_{\mathrm{T}}$ and there is a similar expression for $\tilde{f}$. Substituting these solutions into the expression for the current equation (17) one obtains the following result for magnetic field dependence of the supercurrent

$$I(H,\phi) = I_C(H=0)\int_{-1/2}^{1/2} d\tilde{y}\sin(\phi - 2s\tilde{y}), \tag{22}$$

where ϕ is the non-gauge invariant superconducting phase difference and $I_C(H=0)$ is the critical current at zero field, which is given by (19) with $\Gamma_{\mathrm{H}} = 0$. The previous expression shows that in this limit the only effect of the field is to replace the phase ϕ by the corresponding gauge-invariant combination $\phi - 2s\tilde{y}$. As a consequence, the critical current in the wide junction limit exhibits, as expected, the well-known Fraunhofer pattern which is described by the expression [4]

$$\frac{I_C(H)}{I_C(H=0)} = \frac{|\sin(\pi\Phi/\Phi_0)|}{\pi\Phi/\Phi_0}. \tag{23}$$

The analytical solution of (21) allows us exploring in detail the structure of the superconducting correlations in the normal wire in this limit. Such correlations are described by the pair correlation function of (5). From (21) one can show that this pair correlation function Ψ vanishes in some particular points inside the normal wire in which the electronic structure is not affected by the proximity effect. Such points are located in the positions given by

$$\tilde{x}_0 = 1/2 \quad \text{and} \quad \phi - 2s\tilde{y}_0^{(m)} = (2m+1)\pi, \tag{24}$$

where $m = 0, \pm 1, \ldots$ and $\tilde{y} \in [-1/2, 1/2]$. This means that in the middle of the N region we find an array of normal cores along the y-direction separated by a distance Φ_0/HL. Notice also that the phase difference ϕ simply shifts rigidly the line of normal cores along the y-direction. Moreover, from (17, 21) one can easily verify that the current density vanishes at these points.

The fact that both Ψ and the current density vanish at those special points suggests that these points are nothing else than the cores of magnetic vortices. In order to demonstrate that this is indeed the case, we proceed to show that the phase of the pair correlation function experiences a 2π jump by integration over any closed contour around the core, which is really the property that defines a vortex. For this purpose, we expand the pair correlation function around one of the points $(\tilde{x}_0, \tilde{y}_0^{(m)})$ given by (24). Following (5), we can now express the pair correlation function as $\Psi = k_{\mathrm{B}}T\sum_n f(\omega_n)$. Thus, we obtain (*cf.* (21))

$$\Psi(\tilde{x},\tilde{y}) = A(\tilde{x}-\tilde{x}_0) + iB(\tilde{y}-\tilde{y}_0^{(m)}), \tag{25}$$

where

$$A = 2(-1)^{m+1} k_B T \sum_{\omega_n} C_n \lambda \sinh(\lambda/2);$$
$$B = 2(-1)^{m+1} s k_B T \sum_{\omega_n} C_n \cosh(\lambda/2), \tag{26}$$

and $C_n = i f_S/(\pi r \lambda \sinh \lambda)$. We see that the function around the point $(\tilde{x}_0, \tilde{y}_0^{(m)})$ can be represented as $\Psi \sim |\Psi| e^{i\theta}$, where $\theta = \tan^{-1}(Bx/Ay)$ (we have shifted the coordinates center to the point $(\tilde{x}_0, \tilde{y}_0^{(m)})$). This means that the phase varies by 2π after any integration around these points, *i.e.* these are vortices with topological charge equal to 1. Moreover, the magnetic flux enclosed in a rectangle delimited by lines in the x-direction half way between two normal cores and two vertical lines inside the electrodes is equal to one flux quantum. Thus, the properties of these vortices are the same as those of the Abrikosov ones. The only difference with the vortices in a bulk superconductor of type II is that the vortices found here are arranged in one-dimensional array instead of forming a two-dimensional lattice [17, 18].

In the light of these results we see that the appearance of the Fraunhofer pattern in the critical current is closely related to the existence of an array of vortices in the center of the N region, in analogy with the situation that takes place in a Josephson tunnel junction. As explained in the introduction, in this latter case the Frauenhofer pattern is due to the so-called Josephson vortices [4]. Obviously, the vortices found in this work are a reminiscence of these Josephson vortices, but with the essential difference that they do possess normal cores. This property is essential to have a complete analogy with the Abrikosov vortices in a type II superconductor.

3.3 Arbitrary Aspect Ratio

So far we have studied the weak proximity regime in the cases where the width was either much smaller or much larger than the magnetic length ξ_H. In the first case (narrow-junction limit), we have shown that the critical current decays exponentially with the magnetic field (see (19)), while in the second (wide-junction limit), it exhibits a Fraunhofer interference pattern (see (23)). In this section we discuss briefly how the critical current interpolates between these two behaviors within the weak proximity regime. For this purpose, we have solved numerically (13, 14) for arbitrary ratio between the width and the length of the normal wire.

In Fig. 3 we show the critical current as a function of the magnetic flux for a wire of length $L = 8\xi$, which is a typical value in the experiments, and different values of the width W. Notice that when $W \sim \xi$ or smaller, which corresponds to the case where the width is clearly smaller than ξ_H, the critical current decays monotonically and it does not exhibit any interference pattern. Indeed, in this case the curves agree nicely with the result of (19). As the width increases, one observes the appearance of an interference pattern in the sense that there are values of the magnetic flux for which the critical current vanishes. It is important to notice that these values are clearly larger than Φ_0 for intermediate widths and the patterns are not really "periodic". Then, when the width is comparable to the length (see curve for $W = 10\xi$) the interference pattern approaches the standard Fraunhofer pattern with zeros at multiples of Φ_0. This pattern is accurately reproduced when $W \gg L$ (see inset of Fig. 3).

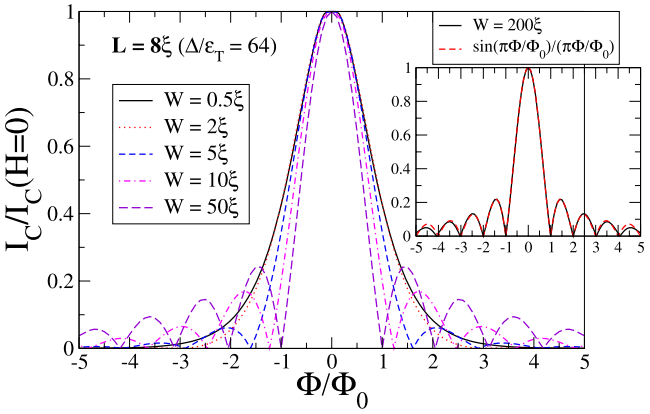

Fig. 3 (Color online) Critical current vs. magnetic flux in the weak proximity limit for a wire length $L = 8\xi$ and a temperature $k_B T = 0.01\Delta$. The different *curves* correspond to different values of the width of the wire, W. The *inset* shows a comparison between the critical current for a width $W = 200\xi$ and the Fraunhofer function of (23)

4 The Vortex State for Transparent Junctions

In this section we shall discuss the results for the case of perfectly transparent interfaces, which are more relevant for a direct comparison with the recent experiments. The analysis of this regime requires the numerical solution of the Usadel equation (2) for arbitrary aspect ratio, a task that we have performed following the steps explained in detail in Sect. 2. We shall start in Sect. 4.1 with an analysis of the local density of states in the normal wire, which turns out to be strongly modulated by the magnetic field, especially in the regime where the vortex structure is fully developed (wide-junction limit). Then, we shall continue in Sect. 4.2 with a detailed study of the pair correlation function in the normal region as a way to elucidate the existence and properties of the magnetic vortices. Then, we shall finish this section with a discussion of the results for the magnetic field dependence of the critical current for arbitrary aspect ratio (see Sect. 4.3).

Although it is impossible to compute analytically the different properties for perfectly transparent interfaces, one can still make some analytical progress in two limiting cases, which gives a valuable insight. The first one is the narrow-junction limit, where the width W is assumed to be smaller than any other length scale, in particular smaller than ξ_H. As explained in Sect. 3.1, using the gauge $\mathbf{A} = -Hy\hat{x}$ and averaging equation (2) over the transversal direction, one arrives at the following one-dimensional equation

$$\frac{\hbar D}{\pi}\partial_x(\hat{G}^R\partial_x\hat{G}^R) + \epsilon[\hat{\tau}_3, \hat{G}^R] = \frac{\Gamma_H}{2\pi}[\hat{\tau}_3\hat{G}^R\hat{\tau}_3, \hat{G}^R], \tag{27}$$

where let us recall that the magnetic depairing energy is given by $\Gamma_H/\epsilon_T = (\pi\Phi/\Phi_0)^2/6$. These equations, as in the weak proximity regime, are precisely the same equations that describe the effect of a spin-flip mechanism such as magnetic impurities and we have studied extensively their physical consequences in Ref. [32].

The second useful limit is the wide-junction case ($W \gg \xi_{\mathrm{H}}, L$). In this case it is convenient to use the gauge $\mathbf{A} = Hx\hat{y}$. A dimensional analysis (see Sect. 3.2.) shows that in this limit one can neglect the terms where the derivatives with respect to the y-coordinate appear. In this gauge ($\mathbf{A} = Hx\hat{y}$) the magnetic field also disappears from the equation and its only effect is to change the superconducting phase difference ϕ into the gauge-invariant combination $\phi - 2\pi(\Phi/\Phi_0)y/W$. With this result in mind, it is easy to anticipate how the local DOS will be modulated in the normal wire and, more importantly, it shows that in this wide-junction limit one has a Fraunhofer-like pattern in the critical current vs. magnetic field.

4.1 The Local Density of States

Let us start the discussion of the results by analyzing the local density of states in the normal diffusive wire. In the absence of magnetic field it is well-known that the most prominent feature is the presence of a minigap, Δ_g [33–36]. This minigap is determined, among other factors, by the length of the wire, the interface transparency and the superconducting phase difference (for a detailed discussion, see Ref. [32]). In the absence of magnetic field the minigap is the same throughout the normal wire. As a reference, let us say that for perfect transparency and zero phase difference, the minigap scales with the Thouless energy as $\Delta_g \sim 3.1\epsilon_T$ in the long junction limit ($L \gg \xi$). The question is now, how does the magnetic field modify the local DOS in the normal wire?

In order to answer this question we have computed numerically the local DOS in the normal wire following the procedure explained in Sect. 2. In Fig. 4 we show the results for the local DOS in the middle ($x = L/2$) of a wire of length $L = 8\xi$ for different values of the width, $W/\xi = 1, 8, 200$, and the magnetic flux. The local DOS is shown as function of the energy and y-coordinate to see the field modulation due to the magnetic field. Notice first that for a narrow wire, $W = \xi$ (see upper panels), the local DOS is practically independent of the transversal coordinate. Moreover, when the field is not very high, there is still a clearly defined minigap (see upper left panel). However, when the field is increased, the minigap closes and the DOS progressively tends to the one of the normal state. In the opposite limit, when $W \gg L$, the local DOS is strongly modulated along the y-direction. For low fields ($\Phi < \Phi_0$), the minigap is still open throughout the wire, however for higher Φ the minigap changes in a periodic fashion from its maximum value (equal to the value in the absence of field) to exactly zero at well-defined positions where the DOS is indeed the one of the normal state. In the intermediate regime, when W is comparable to L, the magnetic field closes progressively the minigap, but at the same time it modulates the local DOS along the y-direction.

Let us try to understand these results on the basis of the limiting cases discussed above. As it was explained in Sect. 3.1 and at the beginning of Sect. 4, when the wire is sufficiently narrow, one can show that the magnetic field plays the role of a spin-flip mechanism. This pair-breaking mechanism is characterized by a depairing energy, Γ_{H}, that in units of the Thouless energy is equal to $(\pi\Phi/\Phi_0)^2/6$. It is well-known that the minigap is reduced in the presence of a spin-flip mechanism and vanishes for large values of the depairing energy [32, 35]. In particular, Crouzy *et al.* [37] have

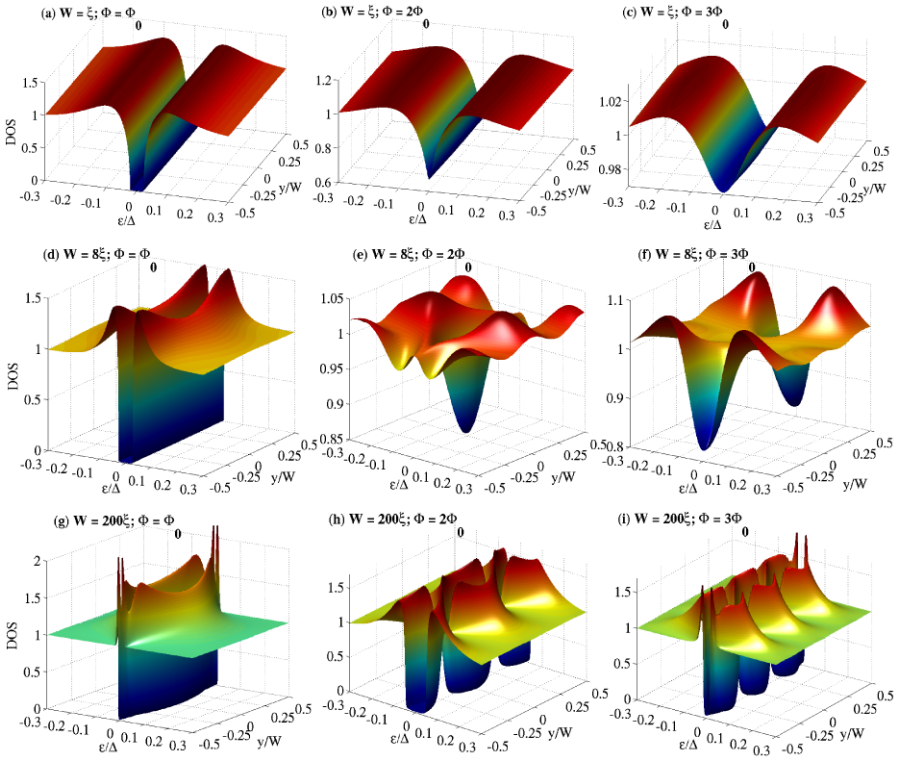

Fig. 4 (Color online) Local density of states as a function of the energy and the y-coordinate in the middle of a wire of length $L = 8\xi$. The different *panels* correspond to different values of the width W and the magnetic flux. The SN interfaces are perfectly transparent and a phase difference $\phi = 0$

shown analytically that in the long junction limit of an SNS structure, the minigap closes at a critical value of $\Gamma_{\mathrm{H}}^{C} = \pi^2 \epsilon_{\mathrm{T}}/2$, i.e. in our case at a critical magnetic flux of $\Phi^{C} = \sqrt{3}\Phi_0$. This explains nicely the results for $W = \xi$ in Fig. 4, where in particular the minigap is already closed for $\Phi = 2\Phi_0$.

In order to explain the results for the case $W = 200\xi$, we remind that in the limit $W \gg L$ the magnetic field only affects the superconducting phase difference, which becomes the gauge-invariant combination: $\phi - 2\pi(\Phi/\Phi_0)y/W$. This means in practice that the different properties of the junction are like in the absence of field, but taking into account that now the local phase depends on the flux and the y-coordinate. It has been shown that when there is a finite phase difference ϕ (in the absence of field) the minigap of a diffusive SNS junction decreases monotonously as ϕ increases and it closes completely when $\phi = \pi$ [36]. This is exactly what happens in the lower panels of Fig. 4. When the gauge-invariant phase difference is equal to zero, the minigap is completely open and reaches the value in the absence of field. However, when this phase is equal to π, the minigap closes. Thus for instance, for $\Phi = 2\Phi_0$ and $\phi = 0$ the gauge-invariant phase is equal to $\mp\pi$ at $y/W = \pm 1/4$, which explains why the local DOS becomes that of the normal states at those positions, see Fig 4(h). It is im-

portant to stress that, although the DOS changes with the x-coordinate, the minigap is independent of x throughout the wire for the same value of the y-coordinate.

Finally, as one can see in the middle panels of Fig. 4, in an intermediate regime, where W and L are comparable, the magnetic field acts at the same time as a pair-breaker and modulates spatially the local DOS in a way similar to what happens in wide junctions.

4.2 The Pair Correlation Function

The peculiar local DOS described in the previous subsection suggests the presence of vortices in the normal wire in wide junctions. This impression was confirmed in the analysis of the weak proximity regime in the previous section and now we proceed to investigate this issue in the case of transparent junctions. For this purpose, we have computed the pair correlation function, $\Psi(\mathbf{R})$, in the normal wire (see (5)). In Fig. 5 we show the modulus of this function (in a logarithmic scale) throughout a wire of length $L = 8\xi$. The different panels correspond to different values of the width and magnetic flux, exactly as in Fig. 4. The common thing in all the panels is the fact that the function diminishes towards the center of the wire, which simply reflects the decay of the superconducting correlations inside the normal wire. What mainly distinguishes the different cases is the modulation of Ψ along the transversal direction. In the case of $W = \xi$ one can see that at low fields (see panel for $\Phi = \Phi_0$), Ψ does not go to zero in the middle of the wire, and for higher fields its value decreases. Moreover, in all the cases there is a negligible modulation of the correlations along the y-direction. In the opposite limit (see lower panels for $W = 200\xi$), one can see how Ψ goes to zero (within the numerical precision) in some points in the middle of the wire ($x = L/2$), which is a signature of the presence of the linear array of vortices discussed in Sect. 3.2. Of course, the number of vortices depends simply on the number of flux quanta in the junction. In the intermediate case (see panels for $W = 8\xi$), the correlations are modulated in the transverse direction, one can already observe the formation of a regular array of vortices.

Let us point out that the position of the vortex cores are determined by (24), which was obtained in the limit of weak proximity effect. This means that the vortex cores are located exactly on the middle of the wire forming a regular line along the y-direction, the center of which depends on the value of the phase difference ϕ. As an example, let us consider the case of $\Phi = 2\Phi_0$. Equation (24) predicts the appearance of two vortex cores located on $y/W = \pm 1/4$, which are exactly the positions that one can read off in the panel of Fig. 5(h). In order to confirm the nature of this magnetic structure for transparent junctions, we have also studied numerically the phase of the pair-correlation function in the case of wide junctions and found that it changes in 2π around any contour that encloses a normal core.

4.3 The Josephson Critical Current

We discuss now the magnetic field dependence of the critical current. In Fig. 6 we show an example for $L = 8\xi$, which is a typical value in the experiments [12], and different values of W. The results are quite similar to those of Fig. 3 for the weak

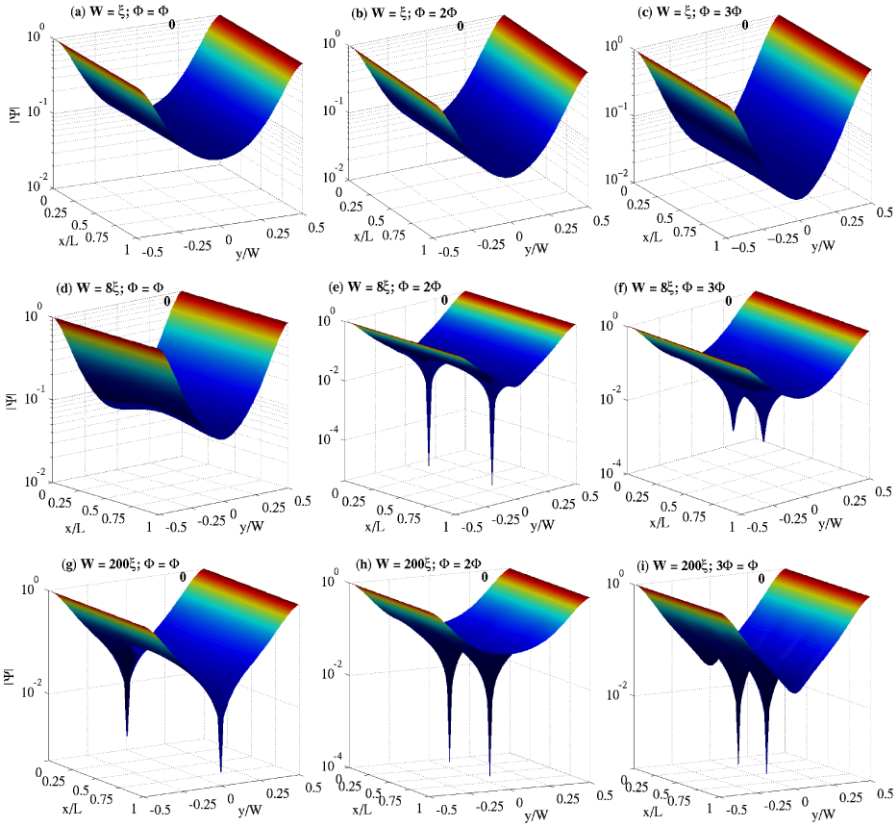

Fig. 5 (Color online) Modulus of the pair correlations, $|\Psi(\mathbf{R})|$, in a wire of $L = 8\xi$ and a phase difference $\phi = 0$. The different panels correspond to different values of the width W and the magnetic flux Φ. $|\Psi(\mathbf{R})|$ has been normalized to its value inside the electrodes and the temperature is $k_B T = 0.01\Delta$. We have assumed perfect transparency for the SN interfaces. Notice the logarithmic scale

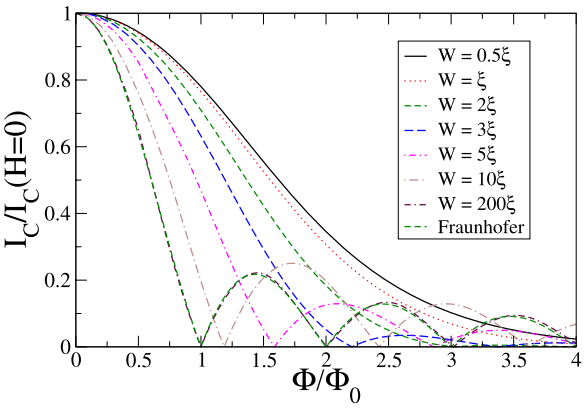

Fig. 6 (Color online) Critical current normalized by the zero-field value vs. magnetic flux for a wire length $L = 8\xi$, perfect transparent interfaces and $k_B T = 0.01\Delta$. The different *curves* correspond to different values of the wire width, W. The *dashed line* shows the standard Fraunhofer pattern given by $\sin(\pi\Phi/\Phi_0)/(\pi\Phi/\Phi_0)$

proximity regime and there are only quantitative differences. First, notice that when $W \sim \xi$ or smaller, and therefore $W < \xi_H$ in the field range shown in the figure, the critical current decays monotonically. As in the weak proximity case, this is simply due to the fact that in this limit no vortices appear, and the field acts as a pair-breaking mechanism that suppresses progressively the superconductivity in the normal wire [32]. Indeed, the curve for $W = 0.5\xi$ agrees quantitatively with the result obtained for the one-dimensional approximation of (27) for the whole range of magnetic field shown in the figure.

As the width increases, one observes the appearance of an interference pattern where the critical current vanishes at certain values of the magnetic flux. Notice that these values are clearly larger than Φ_0 for intermediate widths and the patterns are not really "periodic". Only in the limit $W \gg L$ one obtains a regular pattern with zeros at multiples of Φ_0, recovering the Fraunhofer pattern [3]. These patterns are a consequence of the appearance of the linear array of vortices described above. In particular, in the wide-junction limit the current density in the x-direction is much higher than in the transversal one, and it alternates sinusoidally between the vortex cores, recovering the standard picture of the Josephson vortices. These results explain in an unified manner the different behaviors observed experimentally [5–8, 12], which at first glance seemed to be contradictory.

The agreement between the curve for $W = 200\xi$ and the Fraunhofer pattern (see Fig. 6) might seem surprising, since this latter one corresponds to a junction with a sinusoidal current-phase relation, while this is not the case of our perfect transparent SNS junction at a temperature $k_B T = 0.01\Delta$ lower than the Thouless energy. For this reason, we have studied in more detail the interference pattern in the wide-junction limit ($W \gg L$). It is known that in the absence of magnetic field, the current-phase relationship is non-sinusoidal and can be written as $I(\phi) = \sum_n I_n \sin(n\phi)$. As explained in the introduction of this section, in the wide-junction limit the field only enters in the gauge-invariant phase difference, which immediately leads to the following current-phase relationship

$$I(H, \phi) = \sum_{n=1}^{\infty} I_n \frac{\sin(n\pi \Phi/\Phi_0)}{(n\pi \Phi/\Phi_0)} \sin(n\phi). \tag{28}$$

Notice that the magnetic field dependence in this limit can be calculated in terms of the Fourier coefficients, I_n, in the absence of field. The dependence of these components on the wire length and temperature has been studied in detail in Ref. [38]. If only the term containing I_1 contributed, one would recover exactly the standard Fraunhofer pattern for tunnel junctions. In Fig. 7 we show an example of the interference pattern for a wire length $L = 8\xi$ for different temperatures, ranging from zero temperature to temperatures well above the Thouless temperature. As a reference, we show in the inset the current-phase relationship for the different cases. As it is well-known, below the Thouless temperature the relationship is non-sinusoidal and it becomes sinusoidal for higher temperatures. As one can see in Fig. 7, even at zero temperature the deviations from the standard Fraunhofer pattern for tunnel junctions are indeed rather small. This shows that higher harmonics of the current-phase relationship (I_n with $n > 1$) do not contribute significantly to interference pattern.

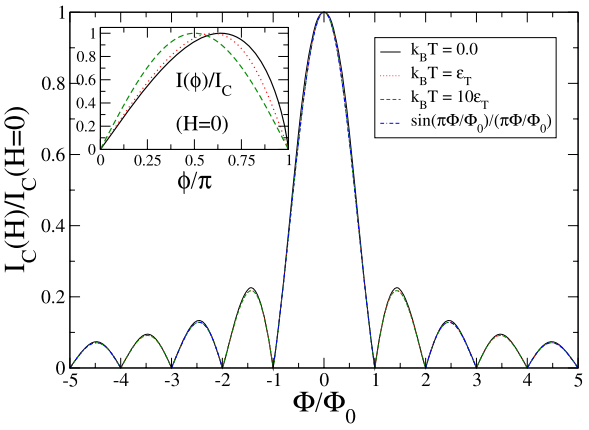

Fig. 7 (Color online) Critical current vs. magnetic flux for a wire with $L = 8\xi$ in the limit $W \gg L$ and comparison with the standard Fraunhofer pattern. The different *curves* correspond to different values of the temperature. We have assumed perfect transparent interfaces. The *inset* shows the corresponding current-phase relationship in the absence of magnetic field for the three different temperatures

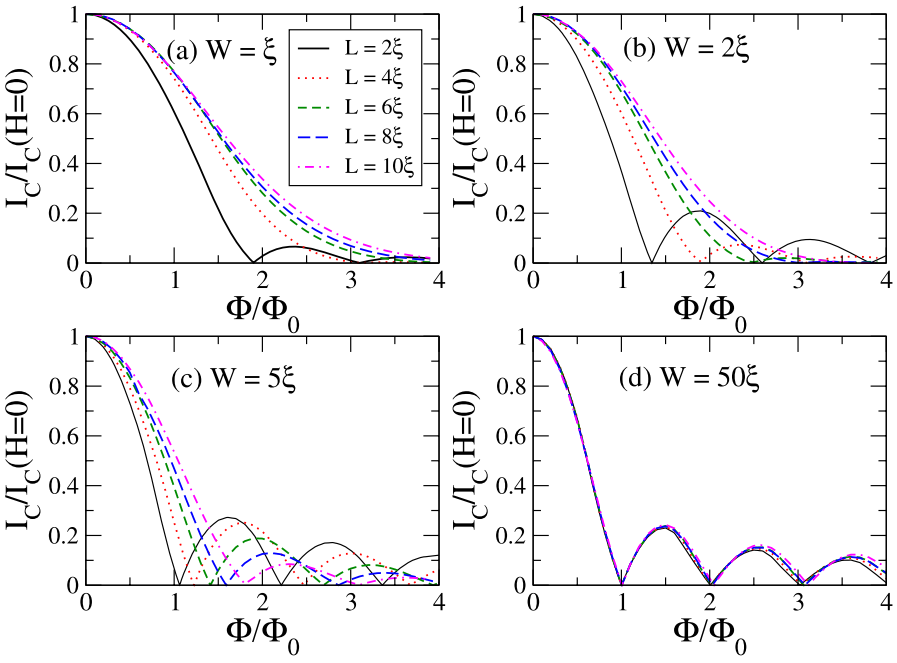

Fig. 8 (Color online) Critical current vs. magnetic flux for different lengths of the normal wire. The different *panels* correspond to different values of the wire width. We have assumed perfect transparent interfaces and $k_B T = 0.01\Delta$

The last issue that we want to address is the role of the length in the crossover between the narrow- and the wide-junction limits. To clarify this issue, we show in Fig. 8 the critical current as a function of the magnetic flux enclosed in the junction for different values of the wire length and width. As one can see, as L increases the appearance of well-defined interference patterns occurs at larger values of W. This confirms the fact that the condition for the appearance of an interference pattern,

i.e. zeros in the critical current, is given, roughly speaking, by $W > \xi_H$, which is equivalent to $W/L > \Phi_0/\Phi$. This means, in particular, that as a simple rule of thumb, one can expect the appearance of the standard Fraunhofer pattern when the aspect ratio becomes of the order of one or larger, i.e. $W \gtrsim L$.

5 Conclusions

In summary, motivated by the recent experiments of Ref. [12] we have revisited in this work the theory of electronic and equilibrium transport properties of a diffusive SNS junction in the presence of a perpendicular magnetic field. Our analysis, based on the quasiclassical theory of superconductivity, provides a complete description of the local density of states and supercurrent for arbitrary aspect ratio (W/L) of the normal wire. We have found that a magnetic vortex structure may develop in the normal metal with properties similar to those in the mixed state of a type II superconductor. This vortex structure is reflected in the appearance of an interference pattern in the critical current that tends to the Fraunhofer pattern in the wide-junction limit ($W \gg \xi_H = \sqrt{\Phi_0/H}$). On the contrary, when W is comparable or smaller than ξ_H, the formation of vortices is not favorable and the field acts as a pair-breaking mechanism which suppresses monotonically the critical current. The vortex structure is also revealed in the strong field modulation of the local density of states (DOS) in the normal wire along the transverse direction. In particular, in the wide-junction limit the local DOS becomes the normal state one at the vortex cores and exhibits a minigap in between those points, the size of which depends on the local value of the gauge-invariant superconducting phase difference.

Our results provide an unified description of the critical current for arbitrary width of the junctions and solve the main puzzle put forward by the experiments of Ref. [12]. Those experiments were performed with samples in the long junction limit ($L \gg \xi$), where the ratio L/W was between 2 and 3 for the junctions with Nb electrodes and it exceeded 7 for the Al junctions. In all cases, a monotonous Gaussian extinction of the critical current at high field was found, which is compatible with our narrow-junction results. However, the quantitative comparison with the experimental results obtained for the widest Nb/Au/Nb was not satisfactory. While the theory predicts the emergence of an interference pattern, the experiments showed a monotonous decay over the whole field range. At the moment the origin of this discrepancy is not understood (for a detailed discussion of the comparison between our theory and the experimental results, see Ref. [12]).

Our theory for the narrow-junction case has also been recently used in another situation. Crosser *et al.* [39] have measured the critical current in a diffusive SNS junction as a function of the magnetic field applied parallel to the current direction. They have found a Gaussian extinction of the critical current similar to that of Ref. [12] for a perpendicular field. The analysis of the Usadel equation [39] shows that a parallel magnetic field can be absorbed into a depairing energy that varies quadratically with the field, in the spirit of (27). Using the scaling $I_C(H)/I_C(H=0) \approx \exp(-0.145\Gamma_H/\epsilon_T)$ for the zero-temperature supercurrent that we obtained in Ref. [32] for narrow junctions, the authors achieved a very good agreement with the experiment.

We propose two kind of experiments to confirm the existence and properties of the vortices predicted in this work. The first one would be a systematic study of the critical current for junctions of varying width. The magnetic field dependence of these junctions should then cross over from a monotonic decay when $W \ll L$ to a Fraunhofer pattern when W approaches L. The second type of experiment would involve a local measurement of the DOS in the normal wire. Obviously, the ideal thing to do would be to use the combined AFM-STM cryogenic microscope of Ref. [40] to obtain local information about this quantity throughout the wire. In particular, it would be desirable to measure the modulation of the local DOS along the transverse dimension due to the field. There is, however, a simpler way to test this modulation. Let us recall that the exact position of the vortex array depends on the value of the phase difference ϕ. Therefore, by controlling the phase, e.g. by passing a supercurrent through the junction, one could modulate the DOS in any given point like for instance in the wire borders. Then, the local DOS at the borders could be measured with the help of an additional probe electrode, in the spirit of the experiments of Refs. [41, 42].

We think that the work presented here paves the way to study the vortex matter in a great variety of hybrid structures. For instance, an ideal two-dimensional system that would be interesting to investigate is the recently introduced superconducting graphene junctions, where a standard Fraunhofer pattern has been observed [43].

Acknowledgements We thank S. Guéron and H. Bouchiat for numerous discussions about their experiments that motivated this work. We also acknowledge useful discussions with P. Joyez, H. Pothier, T.M. Klapwijk and J.G. Rodrigo. This work has been financed by the Spanish CYCIT (contract FIS2005-06255). F.S.B. acknowledges funding by the Ramón y Cajal program.

References

1. B.D. Josephson, Rev. Mod. Phys. **36**, 216 (1964)
2. J.M. Rowell, Phys. Rev. Lett. **11**, 200 (1963)
3. A. Barone, G. Paterno, *Physics and Applications of the Josephson Effect* (Wiley, New York, 1982)
4. M. Tinkham, *Introduction to Superconductivity* (McGraw-Hill, New York, 1996)
5. J. Clarke, Proc. R. Soc. A **308**, 447 (1969)
6. S. Nagata, H.C. Yang, D.K. Finnemore, Phys. Rev. B **25**, 6012 (1982)
7. H.C. Yang, D.K. Finnemore, Phys. Rev. B **30**, 1260 (1984)
8. S.L. Miller, D.K. Finnemore, Phys. Rev. B **30**, 2548 (1984)
9. R. Taboryski et al., Superlatt. Microstruct. **25**, 829 (1999)
10. J. Kutchinsky, PhD thesis, Technical University of Denmark, 2001
11. G. Deutscher, P.G. de Gennes, in *Superconductivity*, ed. by R.D. Parks (Dekker, New York, 1969), p. 1005
12. L. Angers, F. Chiodi, G. Montambaux, M. Ferrier, S. Gueron, H. Bouchiat, J.C. Cuevas, Phys. Rev. B **77**, 165408 (2008)
13. J.C. Cuevas, F.S. Bergeret, Phys. Rev. Lett. **99**, 217002 (2007)
14. J.P. Heida, B.J. van Wees, T.M. Klapwijk, G. Borghs, Phys. Rev. B **57**, 5618 (1998)
15. V. Barzykin, A.M. Zagoskin, Superlatt. and Microstruct. **25**, 797 (1999)
16. U. Ledermann, A.L. Fauchère, G. Blatter, Phys. Rev. B **59**, 9027 (1999)
17. A.A. Abrikosov, Sov. Phys. JETP **5**, 1174 (1957)
18. A.A. Abrikosov, *Fundamentals of the Theory of Metals* (North-Holland, Amsterdam, 1988)
19. V.V. Moshchalkov, V. Bruyndoncx, L. van Look, in *Connectivity and Superconductivity*, ed. by J. Berger, J. Rubinstein (Springer, Berlin, 2001), p. 87
20. V.V. Moshchalkov et al., Nature (London) **373**, 319 (1995)
21. A.K. Geim, I.V. Grigorieva, S.V. Dubonos, J.G.S. Lok, J.C. Maan, A.E. Filippov, F.M. Peeters, Nature (London) **390**, 259 (1997)

22. V.V. Moshchalkov et al., C.R. Physique **7**, 86 (2006)
23. T. Yamashita, L. Rindereer, J. Low Temp. Phys. **21**, 153 (1975)
24. K.D. Usadel, Phys. Rev. Lett. **25**, 507 (1970)
25. A.I. Larkin, Yu.N. Ovchinnikov, in *Nonequilibrium Superconductivity*, ed. by D.N. Langenberg, A.I. Larkin (Elsevier, Amsterdam, 1986), p. 493
26. Yu.V. Nazarov, Superlatt. Microstruct. **25**, 1221 (1999)
27. J. Kopu, M. Eschrig, J.C. Cuevas, M. Fogelström, Phys. Rev. B **69**, 094501 (2004)
28. M. Eschrig, Phys. Rev. B **61**, 9061 (2000)
29. M. Eschrig, J. Kopu, A. Konstandin, J.C. Cuevas, M. Fogelström, G. Schön, Adv. Solid State Phys. **44**, 533 (2004)
30. W.H. Press et al., *Numerical Recipes* (Cambridge University Press, Cambridge, 1992)
31. A.F. Volkov, A.V. Zaitsev, T.M. Klapwijk, Physica C **210**, 21 (1993)
32. J.C. Hammer, J.C. Cuevas, F.S. Bergeret, W. Belzig, Phys. Rev. B **76**, 064514 (2007)
33. A.A. Golubov, M.Yu. Kupriyanov, J. Low Temp. Phys. **70**, 83 (1988)
34. A.A. Golubov, M.Yu. Kupriyanov, JETP Lett. **61**, 830 (1995)
35. W. Belzig, C. Bruder, G. Schön, Phys. Rev. B **54**, 9443 (1996)
36. F. Zhou, P. Charlat, B. Spivak, B. Pannetier, J. Low Temp. Phys. **110**, 841 (1998)
37. B. Crouzy, E. Bascones, D.A. Ivanov, Phys. Rev. B **72**, 092501 (2005)
38. T.T. Heikkilä, J. Särkkä, F.K. Wilhelm, Phys. Rev. B **66**, 184513 (2002)
39. M.S. Crosser, J. Huang, F. Pierre, P. Virtanen, T.T. Heikkilä, F.K. Wilhelm, N.O. Birge, Phys. Rev. B **77**, 014528 (2008)
40. H. le Sueur, P. Joyez, H. Pothier, C. Urbina, D. Esteve, Phys. Rev. Lett. **100**, 197002 (2008)
41. S. Guéron, H. Pothier, N.O. Birge, D. Esteve, M.H. Devoret, Phys. Rev. Lett. **77**, 3025 (1996)
42. A. Anthore, H. Pothier, D. Esteve, Phys. Rev. Lett. **90**, 127001 (2003)
43. H.B. Heersche, P. Jarillo-Herrero, J.B. Oostinga, L.M.K. Vandersypen, A.F. Morpurgo, Nature **446**, 56 (2007)